Contents

Chapter 1 Introduction

1.1 Introduction to SiGe HBTs 1

1.2 Motivation 2

1.3 Thesis outline 4

References 6

Chapter 2 Small-Signal Modeling of III-V HBTs

2.1 Introduction of Small-Signal modeling of III-V HBTs 8

2.2 Origin of Small-Signal Equivalent Circuit of HBTs 8

3.3.1 Derivation of y_{ee} 9

3.3.2 Derivation of y_{ce} 11

3.3.3 Derivation of y_{ec} 13

3.3.4 Derivation of y_{cc} 13

2.3 Common-Emitter y-Parameters of Intrinsic HBT 14

2.4 A Novel Approach for Parameter Determination of HBT Small-Signal Equivalent Circuits 16

3.3.1 Hybrid-π equivalent circuit of the HBT transistor 16

3.3.2 Analytical Determination of the Equivalent Circuit Elements 18

3.3.3 Effect of Extrinsic Elements on Determining Intrinsic Elements 20

3.3.4 The Complete Parameter Extraction Algorithm 21

2.5 Results and Discussions 23

2.6 Summary 24

References 26

Chapter 3 Small-Signal Modeling of SiGe HBTs

3.1 Introduction of Small-Signal modeling of SiGe HBTs 36

3.2 Small-Signal Equivalent Circuit of SiGe HBTs 38

3.3 Small-Signal Modeling of SiGe HBTs 39

3.3.1 Extraction of Extrinsic Elements and Substrate Network Parameters 39

3.3.2 Extraction of Intrinsic Circuit Elements 43

3.3.3 Extraction of of R_{bi}, C_{bci}, C_{π}, and C_{bcx} 44

3.3.4 Accuracy Improvement of R_{bi}, C_{bci} and C_{bcx} 46

3.3.5 Extraction of R_{π}, g_{m0} and τ 47

3.4 Results and Discussions 48

3.5 Summary 49

References 51

Chapter 4 An Analysis of Base Current Effect on the Anomalous Dip of Scattering Parameter S_{12} in SiGe HBTs

4.1 Introduction of Anomalous Dip of Scattering Parameter 71

4.2 S_{12} versus Base Current 72

4.3 Expressions of Scattering Parameters S_{12} 73

4.4 Results and Discussions 76

4.5 Summary 79

References 80

Chapter 5 Computation of Four Noise Parameters Using Genetic Algorithm

5.1 Introduction of Noise Parameters 88

5.2 Determine the Noise Parameters 90

5.3 Optimization Using GAS 91

5.4 Results and Discussions 94

5.5 Summary 95

References 96

Chapter 6 Extraction of Base Current Noise, Collector Current Noise and Their Correlation of SiGe HBTs

6.1 Introduction of Noise Source Extraction 103

6.2 Four-Port Parasitic De-embedding Theory 104

6.3 Four-Port Noise De-embedding Theory 105

6.4 Calculation of 4×4 Four-Port Y matrix of DUT 107

6.4.1 Operand Definition 108

6.4.2 Calculation of Y_{ee} and Y_{ii} 109

6.4.3 Calculation of Y_{ei} and Y_{ie} 111

6.5 Results and Discussions 113

6.6 Summary 117

References 118

Chapter 7. Conclusions

Vita (Chinese)

Publication List

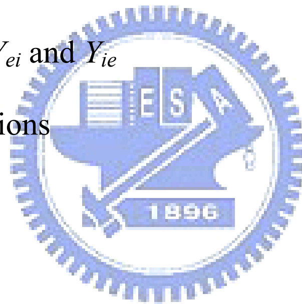

Table Captions

Chapter 2

Table 2.1 Extracted model parameters for the bias condition of V_{CE} = 1.5 V and I_B = 300 μA, 400 μA, 500 μA and 600 μA.

Chapter 4

Table 4.1 Extracted extrinsic elements of the small-signal SiGe HBT model.

Table 4.2 Extracted intrinsic elements of the small-signal SiGe HBT model for the bias condition of I_B = 237 μA, 79.6 μA, and 17.2 μA.

Table 4.3 Expressions of poles and zeros of output impedance ratio and feedback network by dominant pole (zero) approximation

Figure Captions

Chapter 2

Fig. 2.1 Cross section of III-V HBTs.

Fig. 2.2 HBTs biased in the common-base configuration.

Fig. 2.3 Schematic diagram of the small-signal current flows biased in the common-base configuration.

Fig. 2.4 (a) Two-port circuit representation using Y-parameters. (b) A small-signal HBT model based on the circuit representation of Fig. 2.4(a).

Fig. 2.5 Small-signal equivalent circuit of III-V HBTs.

Fig. 2.6 Small-signal equivalent circuit model of intrinsic III-V HBT in common collector configuration.

Fig. 2.7 Frequency characteristics of the intrinsic π-topology parameter C_π with L_C as parameter. The HBT is biased at V_{CE} = 1.5 V, I_B = 600 μA and I_C = 40 mA.

Fig. 2.8 Complete parameter extraction algorithm of proposed method.

Fig. 2.9 Comparison of the measured and calculated S-parameters for the bias point at V_{CE} = 1.5 V, I_C = 17.3 mA, and I_B = 300 μA.

Chapter 3

Fig. 3.1 Cross section of SiGe HBTs.

Fig. 3.2 Small-signal equivalent circuit model for a SiGe HBT in the forward active region.

Fig. 3.3 (a) Small-signal equivalent circuit model for a SiGe HBT biased at V_{BE} = 0 V and forward and/or low reverse collector voltage after de-embedding the "open" dummy pad and removing the extrinsic inductances, extrinsic base

resistance and extrinsic collector resistance. (b) Application of the T↔Π transformation to the HBT device equivalent circuit shown in (a).

Fig. 3.4 Frequency dependencies of the extracted (a) R_{bi} and (b) ωC_π for a SiGe HBT biased at V_{BE} = 0 V and V_{CE} = 3 V.

Fig. 3.5 Plot of Re($Y_{11,k}$) versus ω^2 for the calculation of C_{bci} for a SiGe HBT biased at V_{BE} = 0 V and V_{CE} = 3 V.

Fig. 3.6 Comparison between Y_{sub} and $Y_{22,k}$ + $Y_{21,k}$ for a SiGe HBT biased at V_{BE} = 0 V and V_{CE} = 0 V, 3 V (a) Re(Y_{sub}) and Re($Y_{22,k}$ + $Y_{21,k}$). (b) Im(Y_{sub}) and Im($Y_{22,k}$ + $Y_{21,k}$).

Fig. 3.7 Frequency dependence of the extracted Re(Y_{sub}) and Re($Y_{22,k}$ + $Y_{21,k}$) for three SiGe HBTs with different emitted width (0.34 μm, 0.5 μm, 0.8 μm) biased at V_{BE} = 0 V and V_{CE} = 3 V.

Fig. 3.8 Collector-voltage dependence of the extracted C_{sub}, R_{bk} and C_{bk} for a SiGe HBT biased at V_{BE} = 0 V. Solid line gives the empirical fitting for C_{sub}.

Fig. 3.9 Cross section view of a simple N+-P junction.

Fig. 3.10 Small-signal equivalent circuit model of intrinsic SiGe HBT in common collector configuration.

Fig. 3.11 Plot of Re($A_{c,12}/A_{c,22}$) and Re($A_{c,12}/|A_c|$) versus frequency. V_{BE} = 0.83 V, V_{CE} = 3 V, I_C = 1.333 mA, and I_B = 7.915 μA.

Fig. 3.12 Plot of Im($A_{c,11}$) versus ω. V_{BE} = 0.83 V, V_{CE} = 3 V, I_C = 1.333 mA, and I_B = 7.915 μA.

Fig. 3.13 Plot of Im($A_{c,12}/|A_c|$) versus 1/ω. V_{BE} = 0.83 V, V_{CE} = 3 V, I_C = 1.333 mA, and I_B = 7.915 μA.

Fig. 3.14 Plot of Im($A_{c,11}/A_{c,21}$) versus 1/ω. V_{BE} = 0.83 V, V_{CE} = 3 V, I_C = 1.333 mA, and I_B = 7.915 μA.

Fig. 3.15 Frequency dependence of extracted $1/R_\pi$ for a SiGe HBT biased at V_{BE} =

0.83 V, V_{CE} = 3 V, I_C = 1.333 mA and I_B = 7.915 μA.

Fig. 3.16 Frequency dependence of extracted g_{m0} and τ for a SiGe HBT biased at V_{BE} = 0.83 V, V_{CE} = 3 V, I_C = 1.333 mA and I_B = 7.915 μA.

Fig. 3.17 Measured (Symbol) and simulated (line) S-parameters of the 3×0.34×8 μm^2 SiGe HBT in the frequency range of 1–30 GHz, at V_{BE} = 0.8 V, V_{CE} = 2 V, I_B = 2.477 μA, and I_C = 0.414 mA.

Chapter 4

Fig. 4.1 (a) Measured scattering parameters S_{12} of a SiGe HBT with emitter size of 1.24×3.2 μm^2 biased at V_{CE} = 2 V and I_B = 237 μA, 79.6 μA, 17.2 μA. (b) The measured scattering parameters S_{12} before and after pad lines and interconnects de-embedded. The measured SiGe HBT is with emitter size of 1.24 ×3.2 μm^2 biased at V_{CE} = 2 V and I_B = 237 μA.

Fig. 4.2 Setup for the measurement of the SiGe HBTs S-parameters. (a) A complete circuit including a small-signal hybrid-π model. (b) A simplified circuit with the local series-series feedback element (R_e) absorbed.

Fig. 4.3 Comparison of the experimental and calculated scattering parameters S_{12} of a SiGe HBT with emitter size of 1.24×3.2 μm^2 biased at V_{CE} = 2 V and I_B = 79.6 μA.

Fig. 4.4 Measured and modeled S-parameters of a SiGe HBT with emitter size of 1.24×3.2μm^2 biased at V_{CE} = 2 V and I_B = 79.6 μA.

Fig. 4.5 Frequency response of the phase of the scattering parameters S_{12} of a SiGe HBT with emitter size of 1.24×3.2 μm^2. (a) The SiGe HBT is biased at V_{CE} = 2 V and I_B = 237 μA. (b) The SiGe HBT is biased at V_{CE} = 2 V and I_B = 17.2 μA.

Chapter 5

Fig. 5.1 Estimated error ε_i for the proposed method. The lines designated by ε_L and ε_M, represent the corresponding error function used in the conventional method [1], [2], respectively.

Fig. 5.2 Schematic flowchart of the GA used in this work.

Fig. 5.3 Sum of error as a function of generation number for determination of noise parameters using genetic algorithms.

Fig. 5.4 Computation time as a function of number of measured source impedance. The computation of both methods are performed on a AMD-1.3GHz computer.

Fig. 5.5 The computed noise parameter standard deviation as a function of the number of measured source impedance. Circle: Mitima method, Triangle: Proposed method and Square: Vasilescu method.

Fig. 5.6 Calculated four noise parameters using proposed computation method.

Chapter 6

Fig. 6.1 Illustration of a general four-port structure. The two extrinsic ports of the DUT are denoted ports 1 and 2, and the two ports of intrinsic device (INT) are denoted ports 3 and 4.

Fig. 6.2 Equivalent circuit of the noise model of the DUT. Here, i_{n1}, i_{n2} , i_{n3} , and i_{n4} are noise current sources at ports 1–4, respectively, and $i_{n,int1}$ and $i_{n,int2}$ are the noise current sources of the intrinsic two-port system.

Fig. 6.3 A simple two-port network used for calculating the 4×4 four-port Y-parameters.

Fig. 6.4 Small-signal equivalent circuit of SiGe HBTs and corresponding noise

sources.

Fig. 6.5 Flow chart of extraction of intrinsic noise sources.

Fig. 6.6 Comparison of modeling results extracted from S-parameters measured from HP-8510 with measured S-parameters from ATN-NP5B.

Fig. 6.7 Extracted base current noise versus frequency.

Fig. 6.8 Extracted collector current noise versus collector current.

Fig. 6.9 Extracted collector current noise versus collector current.

Fig. 6.10 Extracted correlation between base current noise and collector current noise.

Fig. 6.11 Measured four noise parameters and calculated four noise parameters based on the proposed model and conventional $2qI_B$, $2qI_C$ assumption.